

The optimization of paths in the $R^{3,1}$ space time by

Markov Chain Monte Carlos

Sadataka Furui^A and Serge Dos Santos^B

^A Faculty of Science and Engineering, Teikyo University

2-17-12 Toyosatodai, Utsunomiya, 320-0003 Japan *

^B INSA Centre Val de Loire; Université de Tours,

INSERM, Imaging Brain & Neuropsychiatry iBrain U1253 F-41034 Blois Cedex, France †

June 24, 2024

Abstract

We propose a method to obtain the optimal weight function of 9 paths in (3+1)D space-time whose length is less than or equal to $2 \times (6 + 2)$ lattice units. The factor 2 comes from inclusion of opposite direction path or time reversed paths. There are 2×2 time shifts, which we assume that they can be regarded as stochastic Markov processes. We prepare the input 9D vector \mathbf{X} and a 9×9 matrix \mathbf{W} and a bias vector \mathbf{b} , and consider affine transformations $\mathbf{Z}^{(h)} = \mathbf{X}^{(in)} \mathbf{W}^{(h)T} + \mathbf{b}^{(h)}$ and $\mathbf{A}^{(h)} = \sigma(\mathbf{Z}^{(h)})$ from an input layer to a hidden layer, the hidden layer to another hidden layer and from the hidden layer to an output layer, using the transformation $\mathbf{Z}^{(x)} = \mathbf{A}^{(h)} \mathbf{W}^{(out)T} + \mathbf{b}^{(x)}$ and $\mathbf{A}^{(x)} = \sigma(\mathbf{Z}^{(x)})$.

By choosing the matrix \mathbf{W} a diagonal matrix, and introducing the information of action of the 9 paths, a simple Monte Carlo simulation yields actions on a 2D plane spanned by e_1, e_2 for a fixed $u_2 = j_2 e_2$ as a function of $u_1 = j_1 e_1$. The action at high momentum region has small fluctuations, but at small momentum region, has large fluctuation. Generalizing \mathbf{W} including mixing of paths, we search the optimal weight function using the Machine Learning (ML) techniques. For fixed point actions, actions of the output layer are defined by the output of final hidden layer

*E-mail address: furui@umb.teikyo-u.ac.jp

†E-mail address: serge.dossantos@insa-cvl.fr

1 Introduction

Recently, application of quaternions in engineering and physics has been intensively discussed[1, 2, 4, 5, 6].

In the Time Reversal Based Nonlinear Elastic Wave Spectroscopy (TR-NEWS), ultrasonic wave profile was expanded in 3rd order polynomials, and the wave strength of each order was mapped to quaternion bases. From convolution of a ultrasonic wave and its time reversed wave, propagating in 2D planes, anomalous scattering positions are searched[9, 10, 11, 12]. Quaternions which are elements of Clifford algebra are applied in signal and image processing[1]. Felsberg and Sommer[2] proposed for producing monogenic signal from (2+1)D signal using quaternions.

Up to (2+1)D, Non Destructive Testing (NDT) using quaternion bases was successful. We called propagation of solitonic wave on a 2D plane spanned by e_1, e_2 as A-type, on a (2+1)D spanned by $e_1, e_2, e_1 \wedge e_2$ as B-type.

In medical image processing, propagation of 3D materials with hysteresis effects are important. Propagation of solitonic wave in (3+1)D, which we call C-type cannot be described by quaternions, and Dirac showed a prescription of applying Lorentz transformation to quaternions[3]. Although Dirac wrote schemes of bi-quaternions is not of any special interest in mathematical theory, as compared to quaternions, it has interesting physical properties.

In Clifford algebra, the mapping $j : \mathbf{R}^{3,1} \rightarrow M_2(\mathbf{H})$ proposed by Garling[27] is

$$j(\mathcal{A}_{3,1}^+) = \begin{pmatrix} a_1 + a_2\mathbf{k} & b_1\mathbf{i} + b_2\mathbf{j} \\ c_1\mathbf{i} + c_2\mathbf{j} & d_1 + d_2\mathbf{k} \end{pmatrix},$$

where a_i, b_i, c_i, d_i ($i = 1, 2$) are real.

In the Quantum Chromo Dynamics(QCD) lattice simulation[16], here are 7 C-type paths. In bi-quaternion bases, there are additional 2 paths along the time direction, and we consider 9 paths.

The 6 paths $L19, L20, L21, L21', L22, L22'$ do not contain the path along the $e_1 \wedge e_2$ at the beginning or the ending, while $L23, L24, L25$ contain the path along the $e_1 \wedge e_2$ at the beginning or the ending, where e_1 and e_2 are the unit vector spanning a 2D plane. The path $L25$ contains the paths along e_1, e_2 and $e_1 \wedge e_2$.

In [15, 34], we considered 7 paths in (3+1)D that contain hysteresis effects. In this work, we

double the length of the paths to be less than or equal to 16 lattice unit and propose a method to detecting hysteresis effect by comparison with experiments.

The paths of 16 steps are summarized in Table 1 and Table 2. In quaternion basis $q = q_0e_0 + q_1e_1 + q_2e_2 + q_3e_3$ and $\bar{q} = q_0e_0 - q_1e_1 - q_2e_2 - q_3e_3$, we take the $\mathbf{x} = xe_1, \mathbf{y} = ye_2, \mathbf{z} = ze_3$, where $q_i, x, y, z \in \mathbf{R}$

Biquaternions are $e_i e_j$ $i, j \in \{0, 1, 2, 3\}$, and when $i, j \in \{1, 2, 3\}$, $e_i e_j = \epsilon^{ijk} e_k$. $\epsilon^{123} = -\epsilon^{213} = 1$, $\epsilon^{312} = -\epsilon^{132} = 1$ and $\epsilon^{231} = -\epsilon^{321} = 1$.

In the Table 1 and 2, the bi-quaternion basis $e_i e_j$ are denoted as ij , directions of the wave front along the path are x, y, z, t . Backward propagations are $-x, -y, -z, -t$.

step	1	2	3	4	5	6	7	8	9	10	11	12	13	14	15	16
L19	x	y	z	t	-z	-t	-x	-y	-x	-y	-z	-t	z	t	x	y
	23	31	12	24	-12	-24	-23	-31	-23	-31	-12	-24	12	24	23	31
L20	x	y	z	t	-z	-y	-x	-t	-x	-y	-z	-t	z	y	x	t
	23	31	12	24	-12	-31	-23	-24	-23	-31	-12	-24	12	31	23	24
L25	x	y	z	t	-x	-y	-z	-t	-x	-y	-z	-t	x	y	z	t
	23	31	12	24	-23	-13	-12	-24	-23	-31	-12	-24	23	13	12	24

Table 1. Directions of the wave front of paths L19, L20, L25

step	1	2	3	4	5	6	7	8	9	10	11	12	13	14	15	16
L21	x	y	z	t	-z	-x	-t	-y	-x	-y	-z	-t	z	x	t	y
	23	31	12	14/24	-12	-23	-34	-13	-23	-31	-12	-14/24	12	23	34	13
L22	x	y	z	t	-z	-x	-y	-t	-x	-y	-z	-t	z	x	y	t
	23	31	12	14/24	-12	-23	-31	-34	-23	-31	-12	-14/24	12	23	31	34
L23	x	y	z	t	-y	-x	-t	-z	-x	-y	-z	-t	y	x	t	z
	23	31	12	14	-31	-23	-24	-12	-23	-31	-12	-14	31	23	24	12
L24	x	y	z	t	-y	-x	-z	-t	-x	-y	-z	-t	y	x	z	t
	23	31	12	14	-31	-23	-12	-24	-23	-31	-12	-14	31	23	12	24

Table 2. Directions of the wave front of paths L21, L22, L23, L24

The 8 steps of $L19, \dots, L25$ are shown in [13]. The 16 steps of these paths are shown in Figs.1,2, 3,4. At balls, time shifts occur. We assume same hysteretic effects occur stochastically in the balls.

The structure of the rest of the article is as follows. In sect.2 we explain the method of obtaining



Figure 1: The path of $L19$ (left) and that of $L20$ (right). Balls are the places where hysteretic time shift occurs.

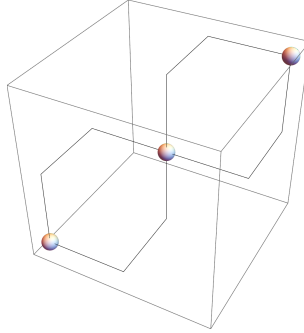


Figure 2: The path of $L25$.

weightfunctions of paths. In sect.3, Markov Chain Monte Carlo is explained. Conclusion and outlook are given in sect.4.

2 Optimization of the weight function by Machine Learning techniques

As in the case of $(2+1)D$, we optimize the weight function of 9 paths ($L19, L20, L21, L21', L22, L22', L23, L24, L25$) in $(3+1)D$ that minimize the path integral action [14].

We adopt a cylindrical lattice model, such that 9 paths start from the origin of a space and returns to the origin. The total action becomes 0 when the path returns to the origin. Therefore at steps 7, 8 and 14,15,16 the action of some path becomes 0.

On the input vector $Y = (y_{19}, y_{20}, y_{21}, y'_{21}, y_{22}, y'_{22}, y_{23}, y_{24}, y_{25})^T$, where T means the transpose, we calculate the integral of action. The $L21$ and $L22$ have direction of wave front along e_1e_4 or



Figure 3: The path of $L21$ (left) and that of $L22$ (right).



Figure 4: The path of $L23$ (left) and that of $L24$ (right).

$e2e4$, and the latter was distinguished by the prime. The optimal weight function is searched using data of j_2 in which action of 9 paths are not zero. For $(u_2/\Delta)/16 = j_2 = 2, 3, 4, 5, 6, 9, 10, 11, 12, 13$, at least one path has non zero action, but action of most paths at $j_2 = 6$ are zero, and at $j_2 = 13$, some paths have problem. We choose 6 steps $j_2 = 4, 5, 9, 10, 11, 12$ which do not contain 0 action component. In $j_2 = 9$ the action of the path $L25$ is exceptionally 0, but we include the path for the optimization. In the case of $j_2 = 3$, action of all paths are equal and we exclude it for the optimization.

Following usual ML algorithms, we define the 9×9 matrix W with 51 random numbers between 0 and 1.

In order to calculate transition matrices X , we first calculate action integral over $u_1/\Delta = i$ ($1 \leq i \leq 255$) at fixed $(u_2/\Delta)/16 = j$.

The training vector is prepared by random numbers as y_1, y_2, \dots, y_9 , 18 replicas, and similar validation vector is prepared with 8 replicas. Replicas mean ordering of random numbers are assigned as in the traveling salesman problem[32, 33].

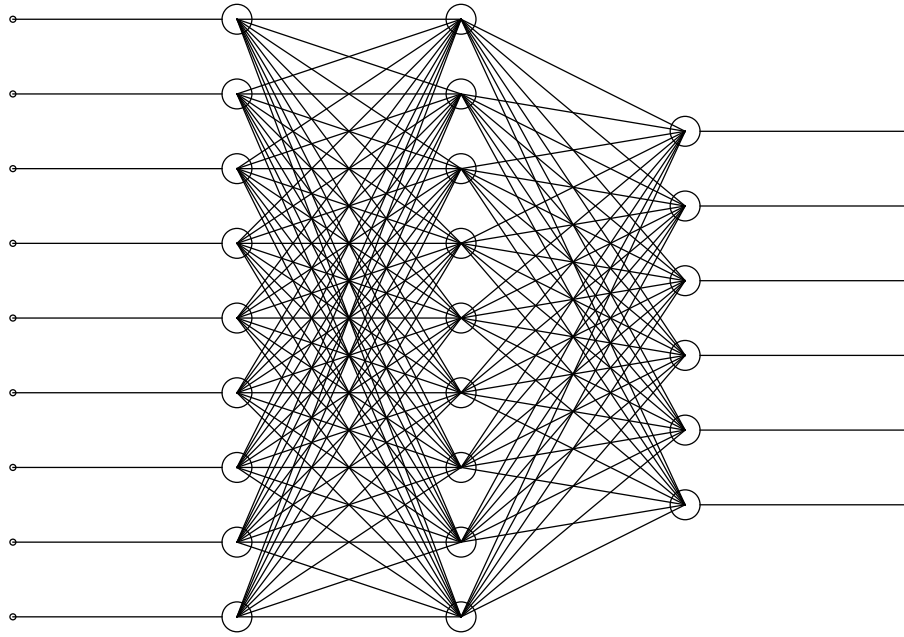


Figure 5: Forward propagating of 9 inputs to 6 outputs through 2 hidden layers in NN. Sources of bias are ignored.

We produce 18 random training vectors which consist of 9 elements that specify the weight of $L19, L20, L21, L21', L22, L22', L23, L24$ and $L25$. We make an inner product of the training vector and the 9 component action integral vector at each step.

Action integrals are calculated as

$$\begin{aligned}
x_1^1 &= \sum_{i=1}^{255} (a19_{4u}(i) + a19_{4d}(i)), \dots, x_6^1 = \sum_{i=1}^{255} (a19_{12u}(i) + a19_{12d}(i)) \\
x_1^2 &= \sum_{i=1}^{255} (a20_{4u}(i) + a20_{4d}(i)), \dots, x_6^2 = \sum_{i=1}^{255} (a20_{12u}(i) + a20_{12d}(i)) \\
x_1^3 &= \sum_{i=1}^{255} (a21_{4u}(i) + a21_{4d}(i)), \dots, x_6^3 = \sum_{i=1}^{255} (a21_{12u}(i) + a21_{12d}(i)) \\
x_1^4 &= \sum_{i=1}^{255} (a21'_{4u}(i) + a21'_{4d}(i)), \dots, x_6^4 = \sum_{i=1}^{255} (a21'_{12u}(i) + a21'_{12d}(i)) \\
x_1^5 &= \sum_{i=1}^{255} (a22_{4u}(i) + a22_{4d}(i)), \dots, x_6^5 = \sum_{i=1}^{255} (a22_{12u}(i) + a22_{12d}(i)) \\
x_1^6 &= \sum_{i=1}^{255} (a22'_{4u}(i) + a22'_{4d}(i)), \dots, x_6^6 = \sum_{i=1}^{255} (a22'_{12u}(i) + a22'_{12d}(i)) \\
x_1^7 &= \sum_{i=1}^{255} (a23_{4u}(i) + a19_{4d}(i)), \dots, x_6^7 = \sum_{i=1}^{255} (a23_{12u}(i) + a23_{12d}(i)) \\
x_1^8 &= \sum_{i=1}^{255} (a24_{4u}(i) + a20_{4d}(i)), \dots, x_6^8 = \sum_{i=1}^{255} (a24_{12u}(i) + a24_{12d}(i)) \\
x_1^9 &= \sum_{i=1}^{255} (a25_{4u}(i) + a21_{4d}(i)), \dots, x_6^9 = \sum_{i=1}^{255} (a25_{12u}(i) + a25_{12d}(i)) \tag{1}
\end{aligned}$$

where $a19_{4u}$ means the action of $L19$ of fixed $u_4/\Delta = 16 \times 4 = 64$, that originates from the large eigenvalue, and $a19_{4d}$ means that originates from the small eigenvalue.

The result of the sum $x_j^1 y_1 + x_j^2 y_2 + \dots + x_j^9 y_9$ for the 6 j_2 show that error bars in the IR region are relatively large, and we optimize the weight function via ML by adopting the affine transformation.

$$X' = XW + b \tag{2}$$

where X is the training vector, b is the bias vector ($b = (b_{19}, b_{20}, b_{21}, b'_{21}, b_{22}, b'_{22}, b_{23}, b_{24}, b_{25})$), and

the matrix W has the form

$$W = \begin{pmatrix} \bullet & * & * & * & * & * & 0 & 0 & 0 \\ * & \bullet & * & * & * & * & 0 & 0 & 0 \\ * & * & \bullet & * & * & * & 0 & 0 & 0 \\ * & * & * & \bullet & * & * & 0 & 0 & 0 \\ * & * & * & * & \bullet & * & 0 & 0 & 0 \\ * & * & * & * & * & \bullet & 0 & 0 & 0 \\ 0 & 0 & 0 & 0 & 0 & 0 & \bullet & * & * \\ 0 & 0 & 0 & 0 & 0 & 0 & * & \bullet & * \\ * & * & * & * & * & * & * & * & \bullet \end{pmatrix} \quad (3)$$

The paths $L19, L20, L25$ returns to the origin in 8 steps. We consider $L21, L21', L22, L22'$ are correlated with $L19, L20$ and $L25$. The paths $L23, L24$ are correlated with $L25$. In the matrix W_{ij} , $1 \leq i, j \leq 9$ specify the path. There are 51 * or \bullet where the random number between 0 and 1 will be assigned.

Hysteresis effects induce difference in actions of $L21$ and $L21'$ and $L22$ and $L22'$ at the step 4 and the step 12. The $L23$ and $L24$ do not contain mixing of $e1e4$ and $e2e4$ and the actions are similar.

The input vector Y is 9 dimensional and we prepare 18 sets for training and 9 sets for validation.

From input $Y^{(in)}$ one gets $Z^{(h)} = Y^{(in)}W^{(h)T} + b^{(h)}$ in the hidden layer, and we activate using the sigmoid function as $A^{(h)} = \sigma(Z^{(h)})$,

$$\sigma(z) = \frac{1}{1 + e^{-z}}$$

The value z is standardized as [28],

$$z_{m,n}^{std} = \frac{z_{m,n} - E(z_{m,n})}{Var(z_{m,n})}$$

where $E(z_{m,n})$ is the average of the set $z_{m,n}$ and $Var(z_{m,n})$ is the variance of the set $z_{m,n}$.

The amplitude on the output layer is obtained by using $Z^{(x)} = A^{(h)}W^{(out)T} + b^{(x)}$ as $A^{(x)} = \sigma(Z^{(x)})$. Here z is standardized by 6 output momenta of $(u_2/\Delta)/16 = 4, 5, 9, 10, 11, 12$. In Figs.6,7,8, the output layer function $A^{(x)}$ of $(u_2/\Delta)/16$ equal 4,5,9,10,11,12, respectively. The color signifies the value of n , for a fixed m . ($1 \leq n \leq 9, 1 \leq m \leq 9$).

Since we want to reduce variations, we take the loss function to be $L = (y - a^{(x)})^2$, where y is the average of $a^{(x)}$ of the one step before.

For three random variables X and Y , one defines [22] the conditional entropy $H(Y|X)$ for the probability $p(x_i) = P(X = x_i)$, $p(y_j) = P(Y = y_j)$, $i = 1, \dots, N$, $j = 1, \dots, M$.

$$H(Y|X = x_i) = - \sum_{j=1}^M p(y_j|x_i) \log p(y_j|x_i)$$

and

$$\begin{aligned} H(Y|X) &= \sum_{i=1}^N p(x_i) H(Y|X = x_i) \\ &= - \sum_{i=1}^N \sum_{j=1}^M p(x_i) p(y_j|x_i) \log p(y_j|x_i) \end{aligned} \quad (4)$$

For random variables X, Y and Z , the Markov chain $X \rightarrow Y \rightarrow Z$ satisfies $p(Z|X, Y) = p(Z|Y)$. It means that the past is essentially conditioned only by the previous variable.

$$\begin{aligned} \frac{\partial L}{\partial w^{(x)}} &= 2(a^{(x)} - y) \frac{\partial a^{(x)}}{\partial z^{(x)}} \frac{\partial z^{(x)}}{\partial w^{(x)}} \\ &= 2(a^{(x)} - y) a^{(x)} (1 - a^{(x)}) a^{(h)} \end{aligned} \quad (5)$$

The bias vector in the output layer is $\eta \frac{\partial L}{\partial b} \sim \eta a^{(x)} (1 - a^{(x)}) a^{(h)}$ where η is a learning rate.

The weight $w^{(x)}$ is updated via stochastic gradient descent update with a learning rate η as

$$w'^{(x)} = w^{(x)} - \eta \frac{\partial L}{\partial w^{(x)}} \quad (6)$$

The weight of 9 paths at $j_2 = 4, 5, 9, 10, 11, 12$ are shown in Figs.6, 7, 8.

The action integral of $L21'$ (4th path) and $L22'$ (6th path) and $L25$ (9th path) are relatively large.

In our model of separating $L19 - L22'$ and $L23 - L25$, the change of action integral by iterations of $A^{(h)}$ and $A^{(x)}$ calculations are not large. In the left side of Fig.9, the integral of the 1st iteration and the 2nd iteration are compared. The latter (blue) and the former (red) almost the same.

In this test run, input is 9 random number sets and output is 6 action integrals. We observed that the output is independent of number of iterations. We need to consider various 9 random

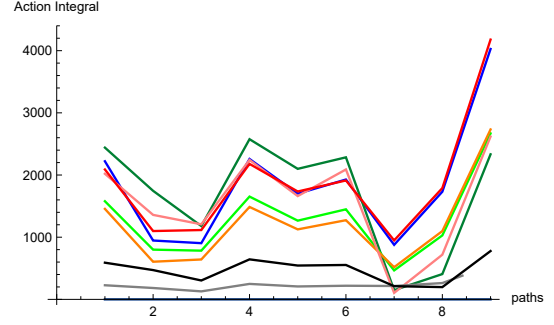
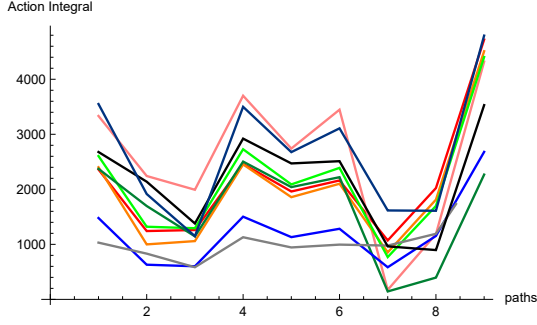


Figure 6: The weight of output 1_0 (left) and that of output 2_0 (right).

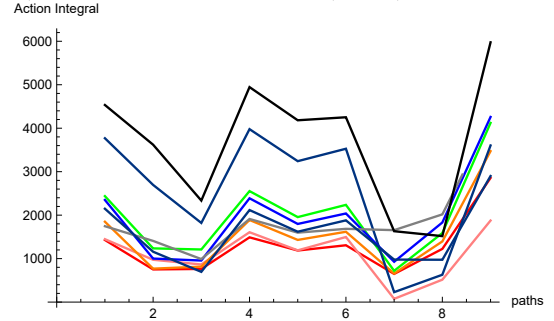
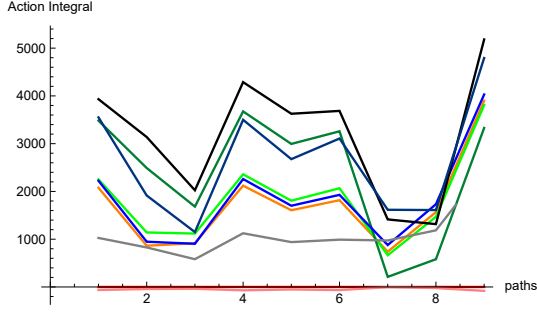


Figure 7: The weight of output 3_0 (left), and that of output 4_0 (right).

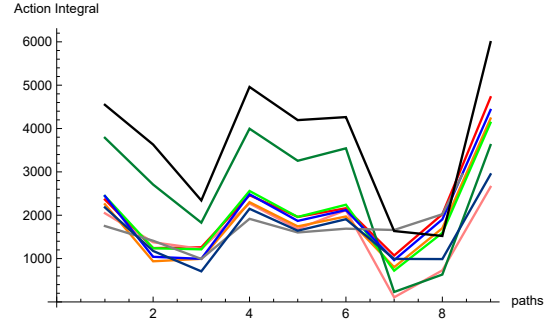
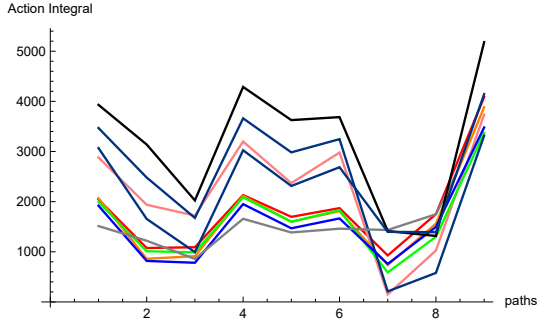


Figure 8: The weight of output 5_0 (left), and that of output 6_0 (right).

number sets and obtain hidden layer sets, choose 51 parameters for the transition between the 9 channel hidden layers and calculate output-layer sets The optimal weight function could be obtained by searching the set that yields minimal action.

3 Markov Chain Monte Carlo

One defines the transition probability of Markov process $X(t)$ as $F(t, x; u, E)$, which has the following property [18],

- 1) For arbitrarily fixed t, u, x , it is a measurable distribution of $x \in E$.

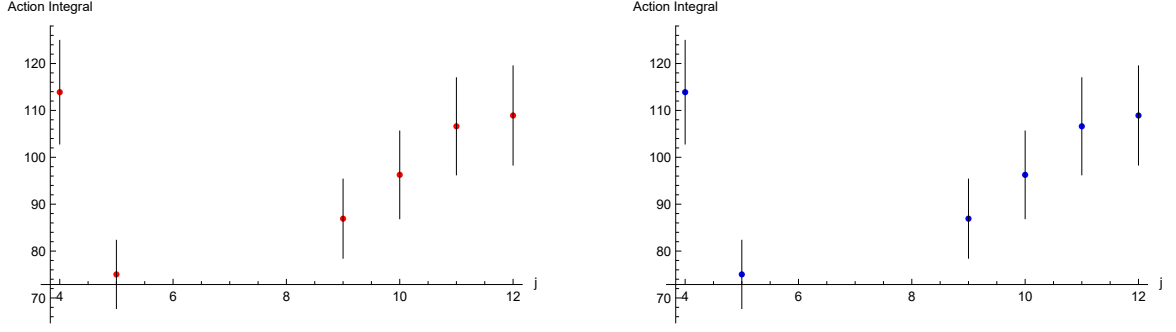


Figure 9: Action integral of the 1st iteration (left), and that of the 2nd iterations (right). They are identical. Error-bars originate from 9 random number set.

$$F(t, x; t, E) = \begin{cases} 1 & (E \ni x) \\ 0 & (E \not\ni x) \end{cases} \quad (7)$$

2) For a fixed $t, u, E, x \in E$ and $t < u < v$, it satisfies the Chapman equation

$$F(t, x; v, \cdot) \simeq \int F(t, x; u, dy) F(u, y; v, \cdot), \quad (t < u < v) \quad (8)$$

One fixes t, x and considers $\varphi_s(E) = F(t, x; s, E)$, ($s \geq t$), and $f_s(x) = F(t, x; s, E)$, ($t \leq s$). We assume that the path in time direction at a fixed lattice point can be approximated by the Markov process, whose transition probability is $F(t, x; s, E)$ and generators A_t, A_t^* .

One defines the forward equation

$$\frac{d\varphi_s(E)}{ds} = (A_s^* \varphi_s)(E) \quad (9)$$

and the backward equation

$$\frac{df_t}{dt} = -A_t f_t. \quad (10)$$

When $X(t)$ is defined at $S = \{1, 2, \dots, r\}$, $A(t)$ is expressed by a matrix $(\alpha_{ij}(t))$ $A^*(t)$ is expressed by its transposed matrix. $\alpha_{ij}(t)$ satisfy stochastic differential equations.

Ito[18] showed that the stochastic integral equation

$$X(t) \simeq X(t_0) + \int_{t_0}^t a(\tau, X(\tau)) d\tau + \int_{t_0}^t b(\tau, X(\tau)) dB(\tau) \quad (11)$$

can be applied to Markov processes. Here $a(\tau, X(\tau))$ and $b(\tau, X(\tau))$ are related to

$$dX(t) = a(t, X(t)) dt + b(t, X(t)) dB(t), \quad t_0 \leq t \leq t_1 \quad (12)$$

and $B(t)$ is the random walk Wiener process in $t_0 \leq t \leq t_1$

τ originates from the modification of $F(t, x; s, y) \ni f$ to $M(a, b, B, \Xi) \ni f$, $(t, s) \subset (a, b)$ and well definedness of

$$\int_t^\sigma f(\tau, \omega) dB(\tau, \omega), \quad t \leq \sigma \leq s. \quad (13)$$

The stochastic mixing of 9 paths in the hidden layer with hysteresis could be incorporated in $b(t, X(t))dB(t)$, and the path in the 3D space represent the $a(t, X(t))dt$ part. We remark that the Radon-Nykodim's theorem says that in Borel measurable space, additive measurable function $\Phi(E)$ is decomposed to an absolutely continuous function $F(E)$ and singular function $\Psi(E)$ [17]

$$\Phi(E) = F(E) + \Psi(E).$$

In our case proceses containing shifts of Markov time[19] contribute to $\Psi(E)$.

In the Kolmogorov's approach[18, 20], variance $V(X)$ and mean $E(X)$ are defined in Borel measure space

$$\begin{aligned} V(X) &= \int_{\Omega} (X(\omega) - E(X))^2 dP(\omega), \\ E(X) &= \sum_{n=1}^4 a_n P(X = a_n) \end{aligned} \quad (14)$$

in the probability space $\Omega(\mathbf{A}, P)$. The average $E(X)$ and the variance $V(X)$ are defined by the Lebesgue integral[17].

Symmetric random walks of a particle in 1D and 2D, and 3D have large qualitative difference. The propability of a particle returns to the original position in 1D and 2D is 1, but that in 3D is about 0.35[20].

Computation of path integral of QCD using Markov Chain Monte Carlo method and Machine Learning techniques are reported in [23].

4 Data transfer between hidden layers

In this section, we include data transfer between two hidden layers through the coincidence of time shift positions of paths. The technique is similar to the treatment of Recurrent Neural Network (RNN)[28].

We prepare 18 input layer 9D vector at $t = 0$: \mathbf{x}^0 and hidden layer vector $\mathbf{h}^{(0)}$. In RNN, the weight matrix is taken as

- \mathbf{W}_{xh} : The weight matrix between the input $\mathbf{x}^{(i)}$ and the hidden layer \mathbf{h} .
- \mathbf{W}_{hh} : The weight matrix associated with the recurrent edge.
- \mathbf{W}_{ho} : The weight matrix between the hidden layer and output layer.

In [28], the concatenated weight matrix $\mathbf{W}_h = [\mathbf{W}_{xh} : \mathbf{W}_{hh}]$,

$$\mathbf{W}_h = \begin{pmatrix} \bullet & * & * & * & * & * & 0 & 0 & 0 & \circ & \circ & \circ & \circ & \circ & \circ & \circ & \circ & \circ \\ * & \bullet & * & * & * & * & 0 & 0 & 0 & \circ & \circ & \circ & \circ & \circ & \circ & \circ & \circ & \circ \\ * & * & \bullet & * & * & * & 0 & 0 & 0 & \circ & \circ & \circ & \circ & \circ & \circ & \circ & \circ & \circ \\ * & * & * & \bullet & * & * & 0 & 0 & 0 & \circ & \circ & \circ & \circ & \circ & \circ & \circ & \circ & \circ \\ * & * & * & * & \bullet & * & 0 & 0 & 0 & \circ & \circ & \circ & \circ & \circ & \circ & \circ & \circ & \circ \\ * & * & * & * & * & \bullet & 0 & 0 & 0 & \circ & \circ & \circ & \circ & \circ & \circ & \circ & \circ & \circ \\ 0 & 0 & 0 & 0 & 0 & 0 & \bullet & * & * & \circ & \circ & \circ & \circ & \circ & \circ & \circ & \circ & \circ \\ 0 & 0 & 0 & 0 & 0 & 0 & * & \bullet & * & \circ & \circ & \circ & \circ & \circ & \circ & \circ & \circ & \circ \\ * & * & * & * & * & * & * & * & \bullet & \circ & \circ & \circ & \circ & \circ & \circ & \circ & \circ & \circ \end{pmatrix}, \quad (15)$$

the state vector

$$\mathbf{x} = (x_1^{(t)}, x_2^{(t)}, \dots, x_7^{(t)}, x_8^{(t)}, x_9^{(t)}, h_1^{(t-1)}, h_2^{(t-1)}, \dots, h_7^{(t-1)}, h_8^{(t-1)}, h_9^{(t-1)})^T,$$

and the activation of the output unit

$$\mathbf{o}^{(t)} = \sigma(\mathbf{W}_{ho}(\mathbf{h}^{(t)})). \quad (16)$$

are used.

However, since evaluation of \mathbf{b}_h is not trivial, we calculate

$$\mathbf{h}^{(t)} = \sigma([\mathbf{W}_{xh} : \mathbf{W}_{hh}] \begin{bmatrix} \mathbf{x}^{(t)} + \mathbf{b}_x \\ \mathbf{h}^{(t-1)} \end{bmatrix}). \quad (17)$$

The bias vectors is

$$\mathbf{b}_x = (b_x^1, b_x^2, \dots, b_x^7, b_x^8, b_x^9)^T,$$

We take the activations of the hidden units at the time $t = 5, 8, 9, 13, 16, 17$ as

$$\mathbf{h}^{(t)} = \sigma(\mathbf{z}^{(t)}) = \sigma(\mathbf{W}_{xh}(\mathbf{x}^{(t)} + \mathbf{b}_x) + \mathbf{W}_{hh}(\mathbf{h}^{(t-1)})). \quad (18)$$

Since we have input vectors $\mathbf{x}^{(t)}$ and $\mathbf{h}^{(t-1)}$, we don't concatenate matrices, and calculate \mathbf{b}_x .

The weight matrix of hidden layers $\mathbf{W}_{hh}^{(t)}$ depends on time (t). We assume that the element of $\mathbf{W}_{hh}^{(t)}$, denoted as $W_{m,n}^{(t)}$ is not 0 when the direction of the path $m: e_i e_4$ and that of $n: e_j e_4$ coincide. At $t = 4, 7, 8, 12, 15$ and 16 , there are time shift points between different paths.

The interactions between hidden layers depends on whether time shift occurs or not.

$$\mathbf{W}_{hh}^{(4)} = \begin{pmatrix} * & * & 0 & * & 0 & * & 0 & 0 & * \\ * & * & 0 & * & 0 & * & 0 & 0 & * \\ 0 & 0 & * & 0 & * & 0 & * & * & 0 \\ * & * & 0 & * & 0 & * & 0 & 0 & * \\ 0 & 0 & * & 0 & * & 0 & * & * & 0 \\ * & * & 0 & * & 0 & * & 0 & 0 & * \\ 0 & 0 & * & 0 & * & 0 & * & * & 0 \\ 0 & 0 & * & 0 & * & 0 & * & * & 0 \\ * & * & 0 & * & 0 & * & 0 & 0 & * \end{pmatrix} \quad \mathbf{W}_{hh}^{(7)} = \begin{pmatrix} 0 & 0 & 0 & 0 & 0 & 0 & 0 & 0 & 0 \\ 0 & 0 & 0 & 0 & 0 & 0 & 0 & 0 & 0 \\ 0 & 0 & * & 0 & 0 & 0 & 0 & 0 & 0 \\ 0 & 0 & 0 & * & 0 & 0 & 0 & 0 & 0 \\ 0 & 0 & 0 & 0 & 0 & 0 & 0 & 0 & 0 \\ 0 & 0 & 0 & 0 & 0 & 0 & 0 & 0 & 0 \\ 0 & 0 & 0 & 0 & 0 & 0 & * & 0 & * \\ 0 & 0 & 0 & 0 & 0 & 0 & 0 & 0 & 0 \\ 0 & 0 & 0 & 0 & 0 & 0 & * & 0 & * \end{pmatrix} \quad (19)$$

$$\mathbf{W}_{hh}^{(8)} = \begin{pmatrix} 0 & 0 & 0 & 0 & 0 & 0 & 0 & 0 & 0 \\ 0 & * & 0 & 0 & 0 & 0 & 0 & * & * \\ 0 & 0 & 0 & 0 & 0 & 0 & 0 & 0 & 0 \\ 0 & 0 & 0 & 0 & 0 & 0 & 0 & 0 & 0 \\ 0 & 0 & 0 & 0 & * & 0 & 0 & 0 & 0 \\ 0 & 0 & 0 & 0 & 0 & * & 0 & 0 & 0 \\ 0 & 0 & 0 & 0 & 0 & 0 & * & 0 & 0 \\ 0 & * & 0 & 0 & 0 & 0 & 0 & * & * \\ 0 & * & 0 & 0 & 0 & 0 & 0 & * & * \end{pmatrix} \quad \mathbf{W}_{hh}^{(12)} = \begin{pmatrix} * & * & 0 & * & 0 & * & 0 & 0 & * \\ * & * & 0 & * & 0 & * & 0 & 0 & * \\ 0 & 0 & * & 0 & * & 0 & * & * & 0 \\ * & * & 0 & * & 0 & * & 0 & 0 & * \\ * & * & 0 & * & 0 & * & 0 & 0 & 0 \\ * & * & 0 & 0 & 0 & * & 0 & 0 & * \\ 0 & 0 & * & 0 & * & 0 & * & * & 0 \\ 0 & 0 & * & 0 & * & 0 & * & * & 0 \\ * & * & 0 & * & 0 & * & 0 & 0 & * \end{pmatrix} \quad (20)$$

$$\mathbf{W}_{hh}^{(15)} = \begin{pmatrix} 0 & 0 & 0 & 0 & 0 & 0 & 0 & 0 & 0 & 0 \\ 0 & 0 & 0 & 0 & 0 & 0 & 0 & 0 & 0 & 0 \\ 0 & 0 & * & 0 & 0 & 0 & 0 & 0 & 0 & 0 \\ 0 & 0 & 0 & * & 0 & 0 & * & 0 & 0 & 0 \\ 0 & 0 & 0 & 0 & 0 & 0 & 0 & 0 & 0 & 0 \\ 0 & 0 & 0 & 0 & 0 & 0 & 0 & 0 & 0 & 0 \\ 0 & 0 & 0 & 0 & 0 & 0 & 0 & 0 & 0 & 0 \\ 0 & 0 & 0 & * & 0 & 0 & 0 & 0 & 0 & 0 \\ 0 & 0 & 0 & 0 & 0 & 0 & 0 & 0 & 0 & 0 \\ 0 & 0 & 0 & 0 & 0 & 0 & 0 & 0 & 0 & 0 \end{pmatrix} \quad \mathbf{W}_{hh}^{(16)} = \begin{pmatrix} 0 & 0 & 0 & 0 & 0 & 0 & 0 & 0 & 0 & 0 \\ 0 & * & 0 & 0 & 0 & 0 & 0 & * & * & * \\ 0 & 0 & 0 & 0 & 0 & 0 & 0 & 0 & 0 & 0 \\ 0 & 0 & 0 & 0 & 0 & 0 & 0 & 0 & 0 & 0 \\ 0 & 0 & 0 & 0 & * & * & 0 & 0 & 0 & 0 \\ 0 & 0 & 0 & 0 & * & * & 0 & 0 & 0 & 0 \\ 0 & 0 & 0 & 0 & 0 & 0 & 0 & 0 & 0 & 0 \\ 0 & * & 0 & 0 & 0 & 0 & 0 & * & * & * \\ 0 & * & 0 & 0 & 0 & 0 & 0 & * & * & * \end{pmatrix} \quad (21)$$

The low and the column are in the order $L19, L20, L21, L21', L22, L22', L23, L24, L25$ and * indicate time shifts in the own path occur or time shifts that cause mixing of paths occur. The path $L21$ and $L21'$ do not mix, similarly $L22$ and $L22'$ do not mix. We are trying to optimize the path using 18 training sets and 8 validation sets.

4.1 Elman Recurrent Neural Network method

When there are two vectors $\mathbf{x}^{(t)}$ and $\mathbf{h}^{(t-1)}$ as the input, the optimal bias vector \mathbf{b}_h is hard to define. In the Elman Recurrent Neural Network (ERNN) [30], the bias vector for \mathbf{x} denoted as \mathbf{b}_x , and that for \mathbf{h} denoted as \mathbf{b}_h are calculated using $\frac{\partial L}{\partial \mathbf{W}_{xh}}$ and using $\frac{\partial L}{\partial \mathbf{W}_{hh}}$, respectively. In ERNN, there is no back propagation, adopted in the NN of [28].

Choosing the expected value $a_k^{(x)}, a_k^{(h)}$ as the means of the 18 samples of $\mathbf{W}^{(x)}\mathbf{x}$ and $\mathbf{W}^{(h)}\mathbf{h}$, respectively, the loss function is

$$L = \sum_k (y_x - a_k^{(x)})^2 + \sum_k (y_h - a_k^{(h)})^2 \quad (22)$$

$$\begin{aligned} \frac{\partial L}{\partial a_k^{(x)}} &= -2(a_k^{(x)} - y_x), & \frac{\partial L}{\partial a_k^{(h)}} &= -2(a_k^{(h)} - y_h) \\ \frac{\partial a_k^{(x)}}{\partial W_{k,k}^{(x)}} &= \frac{\partial}{\partial W_{k,k}^{(x)}} (a_k^{(h)} W_{k,k}^{(x)} + b_k^{(x)}) = a_k^{(h)}, & \frac{\partial a_k^{(h)}}{\partial W_{k,k}^{(h)}} &= 0 \end{aligned} \quad (23)$$

We ignore variation of $\mathbf{W}_{hh}^{(t)}$ and choose $\mathbf{b}_h^{(t)} = 0$. For the activation we adopt the logistic sigmoid function. The weight function $\mathbf{W}^{(x)}$ is modified as

$$W_{k,k}^{(x)} := W_{k,k}^{(x)} - \eta \left\langle \frac{\partial L}{\partial W_{k,k}^{(x)}} \right\rangle, \quad (24)$$

where $\frac{\partial L}{\partial W_{k,k}^{(x)}} = -2(a_k^{(x)} - y_x)a_k^{(h)}$, and $\langle \frac{\partial L}{\partial W} \rangle$ is an average over 18 samples of $\frac{\partial L}{\partial W}$ in the training process and 8 samples in the validation process. The learning rate parameter η is chosen to be 0.01.

With the new $\mathbf{W}^{(x)}$ we calculate the new \mathbf{z}_h and \mathbf{h}

$$\mathbf{z}_h^{(t)} = \mathbf{W}^{(x)}(\mathbf{x}^{(t)} + \mathbf{b}_x^{(t)}) + \mathbf{W}^{(h)}(\mathbf{h}^{(t-1)}), \quad \mathbf{h}^{(t)} = \sigma(\mathbf{z}_h^{(t)}) \quad (25)$$

or when $\mathbf{W}^{(h)}$ is a null matrix

$$\mathbf{z}_h^{(t)} = \mathbf{W}^{(x)}(\mathbf{x}^{(t)} + \mathbf{b}_x^{(t)}), \quad (26)$$

and calculate the output

$$\mathbf{z}_{out}^{(t)} = \mathbf{W}_{ho}(\mathbf{z}_h^{(t)}), \quad \mathbf{y}_{out}^{(t)} = \sigma(\mathbf{z}_{out}^{(t)}). \quad (27)$$

We start from step 4, $\mathbf{h}^{(4)} = \sigma(\mathbf{W}_{xh}(\mathbf{x}^{(4)} + \mathbf{b}_x^{(4)}))$, and randomly produced 9D vector $\mathbf{h}^{(a)}$. We calculate

$$\mathbf{W}_{xh}\mathbf{b}_x^{(4)} = (2(x_1 - m_1)h_1^{(a)}, \dots, 2(x_9 - m_9)h_9^{(a)})^T, \quad (28)$$

where m_k is the k th component of the mean of $\mathbf{W}_{xh}\mathbf{x}^{(4)}$. $h_k^{(a)}$ is the k th component of the hidden layer vector $\mathbf{h}^{(a)}$.

At the step 5, $\mathbf{h}^{(5)} = \sigma(\mathbf{W}_{xh}(\mathbf{x}^{(5)} + \mathbf{b}_x^{(5)}) + \mathbf{W}_{hh}^{(4)}(\mathbf{h}^{(a)}))$, where

$$\mathbf{W}_{xh}\mathbf{b}_x^{(5)} = (2(x_1 - m_1)h_1^{(a)}, \dots, 2(x_9 - m_9)h_9^{(a)})^T,$$

and $\sigma(\mathbf{W}_{xh}\mathbf{b}_x)$ is calculated for evaluating the necessary shifts.

At the step 6, $\mathbf{h}^{(6)} = \sigma(\mathbf{W}_{xh}(\mathbf{x}^{(6)} + \mathbf{b}_x^{(6)}))$.

At the step 7, $\mathbf{h}^{(7)} = \sigma(\mathbf{W}_{xh}(\mathbf{x}^{(7)} + \mathbf{b}_x^{(7)}))$.

At the step 8, $\mathbf{h}^{(8)} = \sigma(\mathbf{W}_{xh}(\mathbf{x}^{(8)} + \mathbf{b}_x^{(8)}) + \mathbf{W}_{hh}^{(7)}(\mathbf{h}^{(b)}))$, $\mathbf{h}^{(b)} = \sigma(\mathbf{W}_{hh}^{(7)}\mathbf{h}^{(a)})$.

At the step 9, $\mathbf{h}^{(9)} = \sigma(\mathbf{W}_{xh}(\mathbf{x}^{(9)} + \mathbf{b}_x^{(9)}) + \mathbf{W}_{hh}^{(8)}(\mathbf{h}^{(c)}))$, $\mathbf{h}^{(c)} = \sigma(\mathbf{W}_{hh}^{(8)}\mathbf{h}^{(b)})$.

At the step 10, $\mathbf{h}^{(10)} = \sigma(\mathbf{W}_{xh}(\mathbf{x}^{(10)} + \mathbf{b}_x^{(10)}))$.

At the step 11, $\mathbf{h}^{(11)} = \sigma(\mathbf{W}_{xh}(\mathbf{x}^{(11)} + \mathbf{b}_x^{(11)}))$.

At the step 12, $\mathbf{h}^{(12)} = \sigma(\mathbf{W}_{xh}(\mathbf{x}^{(12)} + \mathbf{b}_x^{(12)}))$.

At the step 13, $\mathbf{h}^{(13)} = \sigma(\mathbf{W}_{xh}(\mathbf{x}^{(13)} + \mathbf{b}_x^{(13)}) + \mathbf{W}_{hh}^{(12)}(\mathbf{h}^{(d)}))$, $\mathbf{h}^{(d)} = \sigma(\mathbf{W}_{hh}^{(12)} \mathbf{h}^{(c)})$.

At the step 14 $\mathbf{h}^{(14)} = \sigma(\mathbf{W}_{xh}(\mathbf{x}^{(14)} + \mathbf{b}_x^{(14)}))$.

At the step 15 $\mathbf{h}^{(15)} = \sigma(\mathbf{W}_{xh}(\mathbf{x}^{(15)} + \mathbf{b}_x^{(15)}))$.

At the step 16, $\mathbf{h}^{(16)} = \sigma(\mathbf{W}_{xh}(\mathbf{x}^{(16)} + \mathbf{b}_x^{(16)}) + \mathbf{W}_{hh}^{(15)}(\mathbf{h}^{(e)}))$, $\mathbf{h}^{(e)} = \sigma(\mathbf{W}_{hh}^{(15)} \mathbf{h}^{(d)})$.

At the step 17, $\mathbf{h}^{(17)} = \sigma(\mathbf{W}_{xh}(\mathbf{x}^{(17)} + \mathbf{b}_x^{(17)}) + \mathbf{W}_{hh}^{(16)}(\mathbf{h}^{(f)}))$, $\mathbf{h}^{(f)} = \sigma(\mathbf{W}_{hh}^{(16)} \mathbf{h}^{(e)})$.

At the step 18 $\mathbf{h}^{(18)} = \sigma(\mathbf{W}_{xh}(\mathbf{x}^{(18)} + \mathbf{b}_x^{(18)}))$.

At the step 19 $\mathbf{h}^{(19)} = \sigma(\mathbf{W}_{xh}(\mathbf{x}^{(19)} + \mathbf{b}_x^{(19)}))$.

At the step 20, and at any time t , we calculate the output of 6 selected epochs

$$\mathbf{y}^{(t)} = \mathbf{W}_{ho} \mathbf{h}^{(t)}. \quad (29)$$

where

$$\mathbf{W}_{ho} = \begin{pmatrix} * & * & * & * & * & * & * & * & * \\ * & * & * & * & * & * & * & * & * \\ * & * & * & * & * & * & * & * & * \\ * & * & * & * & * & * & * & * & * \\ * & * & * & * & * & * & * & * & * \\ * & * & * & * & * & * & * & * & * \end{pmatrix} \quad (30)$$

is calculated from the action of 9 paths, and

$$\mathbf{h}^{(t)} = \sigma(\mathbf{W}_{xh}(\mathbf{x}^{(t)} + \mathbf{b}_x^{(t)}) + \mathbf{W}_{hh}^{(t-1)}(\mathbf{h}^{(t-1)})). \quad (31)$$

The iterations of the step 4 to the step 20 continue until the outputs of 18 training samples and 8 validation samples become close together.

Hysteresis increases the action. Parameters of $\mathbf{W}_{hh}^{(t)}$ may be adjusted if experimental data are available. In the present work, non-zero random number denoted by $*$ are created by Mathematica module *RandomReal*[1, k], where k is the number of $*$ in the matrix $\mathbf{W}_{hh}^{(t)}$.

We performed a test run of 20 and 200 iterations of 16 steps, that is starting from the step 4 to the step 16, and return back to the step 1 and proceed until the step 3 makes one round. The

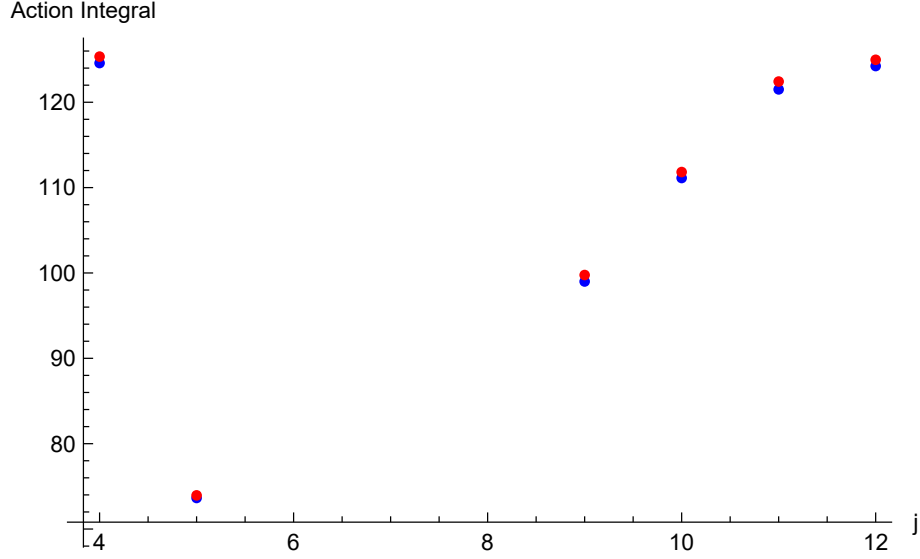


Figure 10: Action integral of the average of 18 training samples with fixed \mathbf{W}_{hh} are blue points and varying \mathbf{W}_{hh} at each round are red points. The coordinate "j" represents the step $j + 16k$ ($k = 0, \dots, \text{itemax} - 1$). The ordinate "Action integral" is the average over itemax data..

Fig.10 is the result of performing 20 iterations using 18 training samples and 8 validation samples. The difference of Action Integral of training samples and validation samples was negligible.

We estimated hysteresis effects by comparing Action Integral using a fixed \mathbf{W}_{hh} through all rounds and creating \mathbf{W}_{hh} at each round. Fig.10 shows the Action Integral of the latter (red points) are slightly larger than the former (blue points).

4.2 Long-Short Term Memory layer method

In recent RNN, long-short term memory (LSTM) layers are used in order to avoid vanishing gradient problem [28, 29]. Although we do not adopt the method in the present work, we explain the method.

One introduces the forget gate \mathbf{f}_t , input gate \mathbf{i}_t and the candidate value $\tilde{\mathbf{C}}_t$

$$\begin{aligned}
 \mathbf{f}_t &= \sigma(\mathbf{W}_{xf}\mathbf{x}^{(t)} + \mathbf{W}_{hf}^{(t)}\mathbf{h}^{(t-1)} + \mathbf{b}_f) \\
 \mathbf{i}_t &= \sigma(\mathbf{W}_{xi}\mathbf{x}^{(t)} + \mathbf{W}_{hi}^{(t)}\mathbf{h}^{(t-1)} + \mathbf{b}_i) \\
 \tilde{\mathbf{C}}_t &= \tanh(\mathbf{W}_{xc}\mathbf{x}^{(t)} + \mathbf{W}_{hc}^{(t)}\mathbf{h}^{(t-1)} + \mathbf{b}_c)
 \end{aligned} \tag{32}$$

In our case, $\mathbf{W}_{xf} = \mathbf{W}_{xi} = \mathbf{W}_{xc}$, $\mathbf{W}_{hf}^{(t)} = \mathbf{W}_{hi}^{(t)} = \mathbf{W}_{hc}^{(t)}$ are random matrices, $\mathbf{x}^{(t)}$ and $\mathbf{h}^{(t)}$ are

9D vectors.

The cell state at time t is defined as

$$\mathbf{C}^{(t)} = (\mathbf{C}^{(t-1)} \odot \mathbf{f}_t) \oplus (\mathbf{i}_t \odot \tilde{\mathbf{C}}_t), \quad (33)$$

and the output gate at $t = 5, 8, 9, 13, 16, 17$ are

$$\mathbf{o}^{(t)} = \sigma(\mathbf{W}_{xo}\mathbf{x}^{(t)} + \mathbf{W}_{ho}^{(t)}\mathbf{h}^{(t-1)} + \mathbf{b}_o). \quad (34)$$

The outputs at other epochs are

$$\mathbf{o}^{(t)} = \sigma(\mathbf{W}_{xo}\mathbf{x}^{(t)} + \mathbf{b}_o). \quad (35)$$

The hidden unit at t is

$$\mathbf{h}^{(t)} = \mathbf{o}^{(t)} \odot \tanh(\mathbf{C}^{(t)}). \quad (36)$$

\odot denotes the element wise multiplication which is known as Hadamard product[46]. The loss function of \mathbf{x}^t is the difference between the input $\mathbf{h}^{(t)}$ and the output $\hat{\mathbf{o}}^{(t)} \cdot \tanh(\mathbf{C}^{(t)})$.

The loss function of $\mathbf{h}^{(t)}$ is evaluated by using softmax function.

$$S_i = \frac{e^{y_i}}{\sum_k e^{y_k}}, \quad \ell = -\log S_m \quad (37)$$

The derivative of S_i with respect to y_j is

$$\frac{\partial S_i}{\partial y_j} = \begin{cases} S_i(1 - S_j) & j = i \\ -S_i S_j & j \neq i \end{cases} \quad (38)$$

Derivative of $\tanh(s)$ with respect to s is

$$\frac{\partial \tanh(s)}{\partial s} = 1 - \tanh^2(s). \quad (39)$$

The iteration stop condition is $(\mathbf{W}_{ho}\mathbf{h}^{(t)} - \mathbf{W}_{xo}\mathbf{x}^{(t)})^2 < \epsilon$, where ϵ is a positive small real number.

The bias vectors $\mathbf{b}_f, \mathbf{b}_i$ are chosen to be 0, \mathbf{b}_c is $\eta(a^{(x)}(1-a^{(x)})a^{(h)} + a^{(h)}(1-a^{(h)})a^{(x)}) < \epsilon$. The application of LSTM, its bi-directional extension (Bi-LSTM) and gated recurrent neural network (GRU)[31, 30] are left for the future.

5 Conclusion and outlook

We showed that the weight function of paths defined by the fixed point action can be optimized by the Elman RNN method. The optimal weight function of the C-type fixed point actions which contain hysteresis effect can be simulated by using the biquaternion basis. We observed stability of the action on the output layer produced from the hidden layers. There are other RNN methods which are left for the future study.

As an extension of the (3+1)D model, mappings in the (4+1)D : $j(\mathcal{A}_{4,1}) \sim M_2(\mathbf{H}) \oplus M_2(\mathbf{H})$ can be considered by bi-quaternion matrices.

$$j(\mathcal{A}_{4,1}) = \begin{pmatrix} x_2\mathbf{i} + x_3\mathbf{j} + x_4\mathbf{k} & -x_1 + x_5 \\ x_1 + x_5 & -x_2\mathbf{i} - x_3\mathbf{j} - x_4\mathbf{k} \end{pmatrix}.$$

The determinant of $j(\mathcal{A}_{4,1})$ is $x_2^2 + x_3^2 + x_4^2 + x_5^2 - x_1^2$. When we identify it as $-X_0^2$ and transform $x_2 \rightarrow X_1, x_3 \rightarrow X_2, x_4 \rightarrow X_3, x_1 \rightarrow X_4$ and $x_5 \rightarrow X_5$, we obtain the relation $X_1^2 + X_2^2 + X_3^2 + X_5^2 - X_4^2 = -X_0^2$, or $X_0^2 + X_1^2 + X_2^2 + X_3^2 = X_4^2 - X_5^2$, that Dirac derived in the Lorentz transformation of quaternions[3].

In the light front quantization of QCD by Srivastava and Brodsky[37], a fixed light-front time $\tau = (t - z/c)/\sqrt{2}$ is introduced. The light-front time corresponds to $(X_4 - X_5)/\sqrt{2}$. For massless particle, propagators are doubly transverse, i.e. with respect to the gauge direction n_μ and the chirality direction k_μ .

The two $M_2(\mathbf{H})$ represent TR symmetric physical fields, and the BRST ghost fields[39] are decoupled.

Lüscher[47] discussed Abelian chiral gauge theories on the lattice using Dirac spinors which consist of two Weyl spinors. Fermion expectation values of any product \mathcal{O} of fields are obtained as

$$\langle \mathcal{O} \rangle_F = w[m] \int D[\psi] D[\bar{\psi}] \mathcal{O} e^{-S_F}, \quad (40)$$

where the fermion action S_F is assumed to take the form

$$S_F = \sum_{k,j} \bar{c}_k M_{kj} c_j, \quad M_{kj} = \sum_{x \in \Gamma} \bar{v}_k(x) D v_j(x). \quad (41)$$

The integration measures are $D[\bar{\psi}] = \prod_k d\bar{c}_k$, $\bar{\psi}(x) = \sum_k \bar{c}_k \bar{v}_k(x)$.

The weight function $w[m]$ is complex and depends on the presence of zero modes. There is an argument of considering a domain wall in $(4 + 1)D$ space-time [48, 49].

In Klebanov's gauge theory [43, 45], and Chemtob's theory [44], $S^5 \sim S^2 \times S^3 \sim T^{1,1} \sim S^3_1 \times S^3_2/U(1)$ i.e. product of two quaternions modulus $U(1)_R$ symmetry. Quaternion Field Theory proposed by Adler [40] and his extension in the frame work of gauge theory [42] has new progress.

Quaternion and bi-quaternion basis model can be used not only for NDT, but also for QCD lattice simulations. For getting the optimal solution, ML techniques can be applied. Nonlinearity and hysteresis could be explored in these basis.

Acknowledgments

S.F. thanks the Laboratory for Industrial Research (Nissanken) for the financial aid to the travel expense to INSA Centre Val de Loire in November 2024 and Prof. S.J. Brodsky for helpful communication. The numerical calculation was done using Mathematica of the Wolfram Research installed on a workstation of the faculty of science and engineering of Teikyo University. S.F. is grateful to Prof. M. Arai and Prof. K. Hamada for the permission.

References

- [1] Miran, S. , Flamant, J. , Le Bihan, N. , Chainais,P. and Brie, D. : Quaternion in Signal and Image Processing, A comprehensive and objective overview, IEEE Signal Processing Magazine **40** (6) (2023).
- [2] Felsberg, M. and Sommer, G. : The Monogenic Signal, IEEE. Trans. Signal Proc. **49** (12) 3136-3144 (2001).
- [3] Dirac, P.A.M.: Application of Quaternions to Lorentz Transformations, Proc. R.I.A. vol. 5 Sect. A 261-270 (1945).
- [4] Unser, M., Sage, D. and Van De Ville, D. , : Multiresolutioion Monogenic Signal Analysis Using the Riesz-Laplace Wavelet Transform, IEEE Trans. Image Proc. **18** (11) (2009).
- [5] Unser, M. and Van De Ville, D. : Wavelet Steerability and the Higher-Order Riesz Transform, IEEE Trans. Image Proc. **19** (3) 636-652 (2010).

- [6] Bridge, C.P. : An introduction to the monogenic signal, arXiv:1703.09199v1 [cs.CV] (2017)
- [7] Dvorakova, Z. , Dos Santos, S. , Kus V. and Prevolovsky, Z. : Localization and Classification of scattered nonlinear ultrasonic signatures in bio-mechanical media using time reversal approach, J. Acoust. Soc. Am. **154** (3) pp.1684-1695 (2023).
- [8] Lopez, A. , Bacelar, R., Pires, I., Santos, T. G., Sousa, J. P. and Quintino, L. : Non-destructive testing application of radiography and ultrasound for wire and arc additive manufacturing, Additive Manufacturing, **21**, 298-306, Elsevier (2018).
- [9] Goursolle, T., Callé, S. , Dos Santos, S. and Bou Matar, O.: A two-dimensional pseudospectral model for time reversal and nonlinear elastic wave spectroscopy, J. Acoust. Soc. Am **122**(6) pp.3220-3229 (2007).
- [10] Dos Santos, S. and Plag, C. ,: Excitation Symmetry Analysis Method (ESAM) for Calculation of Higher Order Nonlinearities, Int. J. Non-Linear Mech. **43** 104-119 (2008).
- [11] Dos Santos, S. : Analyse des symétries pour un traitement du signal systématique: application à l'imagerie non linéaire des milieux complexes, 10ème Congrès Français d'Acoustique, Lyon (2010)
- [12] Lints, M. Salpere, A. and Dos Santos, S. : Formation and Detection of Solitonic Waves in Dilatant Granular Materials: Potential Application for Nonlinear NDT, NDT.net Issue (2014).
- [13] Furui, S. : On the Quadratic Phase Quaternion Domain Fourier Transform and on the Clifford algebra of $R^{3,1}$, arXiv:2310.10680 v4 (2023).
- [14] Feynman, R.P. : Space-Time Approach to Non-Relativistic Quantum Mechanics, Phys. Rev. **20** (2), 367-387 (1948).
- [15] Furui, S. and Dos Santos, S. : Clifford Fourier Transforms in (2+1)D Lattice Simulations of Soliton Propagations, PoS Lattice22, The 39th International Symposium on Lattice Field Theory, 8th-13th August, 2022, Rheinische Friedrich-Wilhelms-Universität Bonn, Bonn, Germany, arXiv:[hep-lat physics.comp-ph]

- [16] DeGrand, T. , Hasenfratz,A. , Hasenfratz,P. and Niedermayer, F. : Non-perturbative tests of the fixed point action for SU(3) gauge theory, Nucl. Phys.**B454** 615-637 (1995): arXiv:9506031[hep-lat].
- [17] Ito, S. : Introduction to Lebesgue Integrals (in Japanese), Shokabou Shoten, Tokyo (1965).
- [18] Ito, K. : The theory of Probability (in Japanese), Iwanami Shoten. Tokyo (1952); revised (1991)
- [19] Ito, K. and McKean,Jr ,H.P. : Potentials and the Random Walk, Illinois Mathematics **40** 119-132 (1958).
- [20] Feller, W. :An Introduction to Probability Theory and Its Applications, vol.I, John Wiley and Sons, New York (1957), (Translated to Japanese by Kawada,T. et al.) Kinokuniya Shoten, Tokyo (1961).
- [21] Dynkin, E.B. and Yushkevich, A.A. : Markov Processes: theorems and problems, translated from Russian by J. S. Wood, Plenum Press, New York (1969).
- [22] Calin, O. : Deep Learning Architectures: A Mathematical Approach, Springer Series in the Data Science (2020).
- [23] Abbott, R. et al, : Practical application of machine-learned flows on gaugefields, PoS Lattice2023 Proceedings, arXiv:2404.11674v1 [hep-lat] (2024).
- [24] Furui, S. and Dos Santos, S.: Application of Quaternion Neural Network to Time Reversal Based Nonlinear Elastic Wave Spectroscopy, INAE, **8** 183-199, (2023).
- [25] Vahlen, K. Th. : Ueber Bewegungen und complex Zahlen, Math. Ann. **55** 585-593 (1902).
- [26] Porteous, L.R. : Clifford Algebras and the Classical Groups, Cambridge University Press (1995).
- [27] Garling,D.J.H. : Clifford Algebras: An Introduction, Cambridge University Press (2011).
- [28] Raschka, S. ,Liu,Y. and Mirjalili,V. : Machine Learning with Pytorch and Scikit-Learn, Packt Publishing (2022).

- [29] Gers, F., Schmidhuber, J. and Cummins, F.: Learning to Forget: Continual Prediction with LSTM, *Neural Computation* **12**,2451-2471 (2000).
- [30] Bianchi, E.M. et al: Recurrent Neural Networks for Short-Term Load Forecasting, Springer Briefs in Computer Science, <https://doi.org/10.1007/978-3-319-70338-1>
- [31] Chung,J., Gulcehre, C. Cho, K. and Bengio, Y. :Empirical Evaluation of Gated Recurrent Neural Networks on Sequence Modeling, arXiv:1412.3555v1 [cs.NE] (2014).
- [32] Percus, A.G. and Martin, O.C. :Finite Size and Dimensional Dependence in the Euclidean Traveling Salesman Problem, *Phys. Rev. Lett.* **76** (8), 1188-1191 (1996)
- [33] Kinzel, W. and Reents G. : Physics by Computer, (Translated from German by Clajus, M. and Freeland-Clajus, B.), Springer, Berlin (1998).
- [34] Furui, S. : Solving Nonlinear Dynamics using Path-integral methods and Machine Learning techniques, - Paths of Phonetic Solitons in (2+1) D , (3+1)D and Paths of Hadrons in (4+2) D space-time-, in preparation.
- [35] Mayergoyz, I. : Mathematical Models of Hysteresis and their Applications, Elsevier, Amsterdam (2003).
- [36] Papouskova, J. , Kus,V. and Dos Santos, S. : Preisach-Mayergoyz space model density identification for nonlinear physical systems: "L-2" and "D-divergence" minimization methods, *Proceedings of Meetings on Acoustics*, **16**, 045018 (2012).
- [37] Srivastave, P.P. and Brodsky, S.J. : Light-front-quantized QCD in the light-cone gauge: The doubly transverse gauge propagator, *Phys. Rev. D* **64** 045006 (2001).
- [38] Srivastave, P.P. and Brodsky, S.J. : Light-front formulation of the standard model , *Phys. Rev. D* **66**, 045019 (2002).
- [39] Becchi, C. , Rouet, A. and Stora, R. : Renormalization of the abelian Higgs-Kibble model , *Commun. Math. Phys.* **42** 127 (1975).

- [40] Adler, S.L. : Quaternionic Quantum Field Theory, Phys. Rev. Lett. **55** (8) 783-786 (1985).
Errata **55** (13) 1430 (1985).
- [41] Adler, S.L. : Quaternionic Quantum Field Theory, Commun. Math. Phys, **104**, 611-656 (1986).
- [42] Adler, S.L. : Generalized quantum dynamics, Nuclear Physics, **B415**, 195-242 (1994).
- [43] Klebanov, L.R. and Tseytlin, A.A. : Gravity Duals of Superstmmetric $SU(N) \times SU(N + M)$ Gauge Theories, Nucl Phys **B578**, 123 (2000) :arXiv hep-th/0002159.
- [44] Chemtob, M. : Kaluza-Klein theory for type *IIB* supergravity on the warped deformed conifold, arXiv:2209.15503v1 [hep-th] (2022).
- [45] Klebanov. I.R. : Confinement and Dimensional Transmutation, Talk in "QCD at 50" UCLA, (2023).
- [46] Hewamalage, H., Bergmeir, C. and Bandara,K.:Recurrentneural Networks for Time Series Forecasting: Current Status and Future Perspective, arXiv:1909.00590v5[cs.LG] (2020).
- [47] Lüscher, M.:Abelian chiral gauge theories on the lattice with Exact gauge invariance, Nucl.Phys. **B 549** 295-334 (1999).
- [48] Kaplan, D.B. : Chiral Gauge Theory at the Boundary between Topological Phases, Phys. Rev. Lett **132**, 141603 (2024).
- [49] Kaplan, D.B. and Sen, S.: Weyl Fermions on a Finite Lattice, Phys. Rev. Lett. **132**, 141604 (2024).